BRESE, N. E. & O'KEEFFE, M. (1991). *Acta Cryst.* B47, 192–197.
BURKHARD, D. J. M., DE JONG, B. H. W. S., MEYER, A. J. H. M. & VAN LENTHE, J. H. (1991). *Geochim. Cosmochim. Acta*, **55**, 3453–3458.
CROMER, D. T. & MANN, J. B. (1968). *Acta Cryst.* A24, 321–324.
JONG, B. H. W. S. DE (1989). *Glass: Ullmann's Encycl. Ind. Chem. A*, **12**, 365–432.
JONG, B. H. W. S. DE & BROWN, G. E. (1980). *Geochim. Cosmochim. Acta*, **44**, 491–511.
MIGGE, H. (1988). *J. Nucl. Mat.* **151**, 101–107.
PASSIER, H. F. (1993). *Ab Initio Molecular Orbital Calculations on Silicate Systems*, 45 pp. Drs Thesis, Utrecht University.
SHELDRICK, G. M. (1976). *SHELX76. Program for Crystal Structure Determination*. Univ. of Cambridge, England.
SPEK, A. L. (1990). *Acta Cryst.* A46, C34.
TRANQUI, D., SHANNON, R. D., CHEN, H. Y., IIJIMA, S. & BAUR, W. H. (1979). *Acta Cryst.* B35, 2479–2487.
VÖLLENKLE, H., WITTMAN, A. & NOWOTNY, H. (1968). *Monatsh. Chem.* **99**, 1360–1371.
WALKER, N. & STUART, D. (1983). *Acta Cryst.* A39, 158–166.

Acta Cryst. (1994). B50, 518–524

Mechanism of Crystal Dendrite Formation in KNO_3

BY L. J. SOLTZBERG, STELLA A. FAPPIANO, LESLEE D. GRIFFITH, LORI E. HIDEK, SHARON A. OFEK AND LUCCI L. SUAREZ

Department of Chemistry, Simmons College, 300 The Fenway, Boston, MA 02115, USA

(*Received* 12 *July* 1993; *accepted* 21 *January* 1994)

Abstract

KNO_3 dendrites grown from thin layers of supersaturated aqueous solution display dendrite branches growing along the ⟨031⟩, ⟨041⟩ and ⟨051⟩ crystallographic directions. These directions do not correspond to faces in normal polyhedral crystals of KNO_3 and, thus, are directions of fast growth in normal crystals. As the growth rate of a normal KNO_3 crystal is increased by cooling the solution, a sharp transition occurs from growth in the [010] direction to growth in one or more of these ⟨0k1⟩ directions. Interference photomicrographs show that this transition is accompanied by a distortion of the concentration field around the crystal, which further accelerates growth along ⟨0k1⟩. We suggest that these two effects constitute a positive-feedback mechanism responsible for dendrite self-organization.

Introduction

Pattern-formation in nature has long been a subject of contemplation (Thompson, 1961). Extensive study of nonlinear dynamics during the past two decades has led to an understanding of pattern formation in a wide variety of systems (see, for example, Nicolis & Prigogine, 1977; Field & Burger, 1985; Thompson & Stewart, 1986). Diverse studies have shown that systems governed by nonlinear dynamical equations are subject to bifurcations in time and/or space as the systems are driven away from equilibrium. Temporal bifurcations lead to oscillatory behavior and spatial bifurcations lead to symmetry-reducing pattern formation; these phenomena are referred to collectively as 'self-organization'.

Perhaps no other inanimate object so embodies the fascination of pattern formation as does a snowflake. The classic lacy snowflake is a dendritic crystal. Dendrite formation has, therefore, been a subject of scrutiny from the perspective of nonlinear dynamics; practical applications of understanding and controlling dendrite formation have also motivated such work (Langer, 1989, 1992). The dynamical approach focuses on the differential equations describing the continuous variables which govern the behavior of a system. For dendrites growing either from the melt or from solution, the principal factors have been taken to be diffusion of either heat or mass, respectively, and surface tension (Ben-Jacob, Goldenfeld, Langer & Schön, 1983). This continuum thermodynamic viewpoint is specifically and intentionally different from a molecular mechanistic perspective (Langer, 1980), although recent theoretical studies have included kinetic anisotropy at the growing crystal surface (Classen, Misbah, Müller-Krumbhaar & Saito, 1991).

Other investigators have sought an understanding of dendrites in the molecular mechanism of crystal growth. Sunagawa (1981, 1987) has summarized earlier work suggesting that the transition from normal to dendritic habit is related to growth mechanism. The key to this change has been taken to be the 'roughening transition' in which growing surfaces of the crystal are converted from smooth to rough by changes in either temperature or supersaturation (Bennema & van der Eerden, 1987).

©1994 International Union of Crystallography
Printed in Great Britain – all rights reserved

In the present work, we focus on the crystallography of the dendritic material. We were led to this approach by earlier observations in our laboratory which indicated a strong influence of crystal structure on the morphology of certain dendritic materials (Soltzberg, Fappiano, Hidek, O'Brien & Suarez, 1992). We now examine the particular relationship of the directions of elongation in the dendrite (which we shall call the 'directions of dendrite growth') to crystal structure. We find that the directions of dendrite growth in KNO_3 correspond to the copious addition of solute on high index planes of relatively low reticular density, while in the growth of normal polyhedral crystals, the bulk of the solute adds on low index planes. We suggest, as others have done, that the transition from normal to dendritic growth habit is related to the growth mechanism. We offer a different explanation as to why this transition occurs and why the change is so sudden; this explanation, interestingly, embodies one of the fundamental principles of self-organization.

Experimental

The principal techniques employed in this work were polarized light microscopy and shearing-interference microscopy. Dendritic crystals of KNO_3 were grown from aqueous solution by cooling. Observation chambers were prepared by joining two microscope slides with a bead of silicone sealant. The initial bead was run along three sides of one slide. Spacers were placed at the two ends of the first slide, while the second slide was pressed into place on the bead, giving approximate control over the chamber depth; the depth used in the work reported here was 0.1 mm. After the sealant had cured for *ca* 1 h, a sample of the desired solution, saturated at an elevated temperature, was introduced into the chamber and the fourth side of the chamber was sealed with a silicone bead.

At the start of an experiment, the sealed slide was held at the desired starting temperature (below the original mounting temperature) so that the solution in the chamber was saturated at the thermostat temperature. The slide was then quickly transferred to a temperature-controlled stage mounted on a Vickers M72 microscope equipped with a video camera and four-head video recorder. In this manner, the supersaturation prevailing during the initial stages of dendrite growth could be controlled by regulating ΔT between the thermostat and the microscope stage. A similar method has been employed by Dougherty, Kaplan & Gollub (1987); these authors compute a dimensionless supercooling, $\Delta = (C_\infty - C_{eq})/(C_s - C_{eq})$, where C_∞ is the concentration of the high-temperature saturated solution before cooling, C_{eq} is the equilibrium concentration of the solution at the low temperature at which the crystal is growing and C_s is the 'concentration' of the solid. The KNO_3 dendrites described here were grown at a dimensionless supercooling of around 0.12. Frames from video tapes of the growing dendrites were captured with a Macintosh FX computer equipped with a video capture board. Time resolution was 1/30 s.

For study of the diffusion field around the growing dendrites, the microscope was outfitted with a Vickers 10x shearing interference objective and matched condenser. This double-beam optical system superimposes an image of the object of interest upon a reference image of the unoccupied field 330 μm away from the object. The light forming these two superimposed images is coherent, so any path difference between the two images produces a characteristic interference color. In the present case, the 'object of interest' is the region of solution immediately surrounding the dendrite tip and the 'unoccupied field' represents solution as yet unaffected by the growth of the crystal. In this manner refractive index variations (and, thus, concentration variations) in the solution around the growing crystal are made visible. Growth sequences imaged with this optical system were recorded and processed as described above.

Results and discussion

Optical orientation of KNO_3*-faceted crystals and dendrites*

The room-temperature crystal structure of KNO_3 is orthorhombic, space group *Pbnm*, with $a = 9.1709$, $b = 6.4255$ and $c = 5.4175$ Å (Wyckoff, 1964). Principal refractive indices are $n_x = 1.3346$ (b axis), $n_y = 1.5056$ (c axis) and $n_z = 1.5064$ (a axis) (Winchell & Winchell, 1964).

Normal faceted crystals of KNO_3 (Fig. 2) were grown at dimensionless supercoolings of about 0.05. These crystals were prisms with morphology corresponding to that reported by Groth (1908). Observation of conoscopic interference figures, together with optic sign determination, confirmed that the observation direction in Fig. 2 is [100] and the long growth direction is [010]. These prisms extinguish sharply on the microscope stage with the prism axes perfectly aligned with the crossed polars. Fig. 7 shows the projection of the KNO_3 structure on (100), for reference.

Dendritic mats of KNO_3 (Fig. 1) were grown at dimensionless supercoolings of about 0.12. *None of the directions of dendrite growth correspond to extinction directions.* In the dendrite mat shown in Fig. 1, there are two directions of dendrite growth, making angles of $+17$ and $-21°$ with the nearest extinction

direction. Thus, the directions of dendrite growth are not the same as the growth directions of faceted KNO_3 crystals, and they do not correspond to axial directions of the unit cell.

Sidebranch angles in KNO_3 dendrites

The sidebranch angles were measured in several locations on numerous frames showing dendritic mats similar to Fig. 1. Sidebranch angles of 42, 38 and 35° were observed in different frames. The angles seen in any one frame were generally quite consistent. The standard deviation of repeated measurement of any one angle on replicate printouts was 0.6°.

Transition from faceted growth to dendritic growth

When the growth rate of a faceted crystal like that shown in Fig. 2 was increased by further cooling, the (010) face began to advance more rapidly. With the interference microscope, a concentration gradient became visible around the advancing crystal (Fig. 3). Further acceleration of the growth rate produced a steeper gradient (Fig. 4). Continued increase in the growth rate was accompanied by a sudden transition (Fig. 5), in which the previously flat advancing face broke into many small discontinuous regions and the outer corners of the face began to advance much more rapidly. Exaggerated growth in this new direction gave either a needle crystal (Fig. 6) or a branched dendrite, depending on the degree of supercooling. We did not attempt to determine a critical degree of undercooling associated with this transition. Qualitatively, it appears that the transition occurs when the growth exceeds a certain rate; presumably, this would be associated with a particular degree of undercooling.

An important feature in Fig. 5 is the shape of the concentration gradient field. As the growth at the corners began to accelerate, the diffusion field

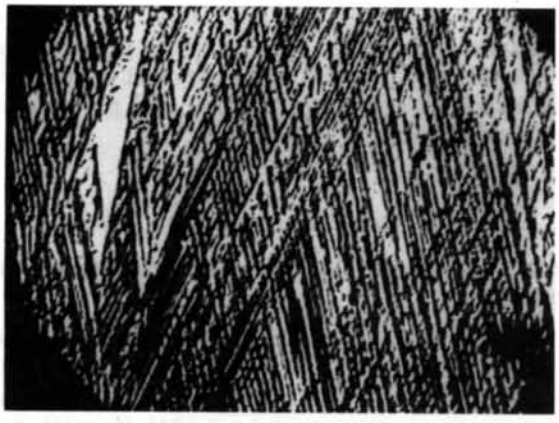

Fig. 1. KNO_3 dendrite mat grown by supercooling from 318 to 288 K. Sidebranch angle = 38°. The long dimension of the photograph equals 1.3 mm.

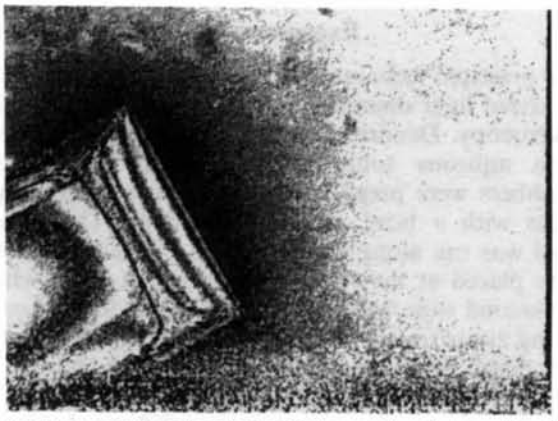

Fig. 3. Same crystal as in Fig. 2 with temperature being reduced to 298 K. Long direction is [010]. The area furthest from the crystal is the region of highest concentration. The long dimension of the photograph equals 0.54 mm.

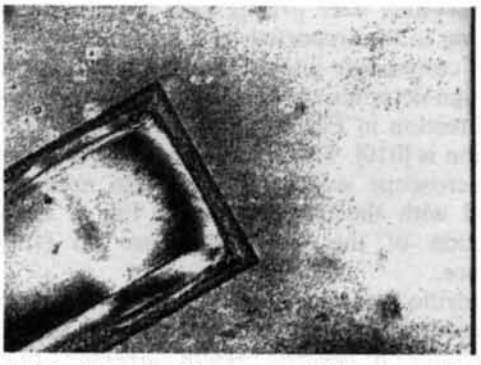

Fig. 2. KNO_3 single crystal grown at 307 K. Long direction is [010]. Area furthest from the crystal is the region of highest concentration. The long dimension of the photograph equals 0.54 mm.

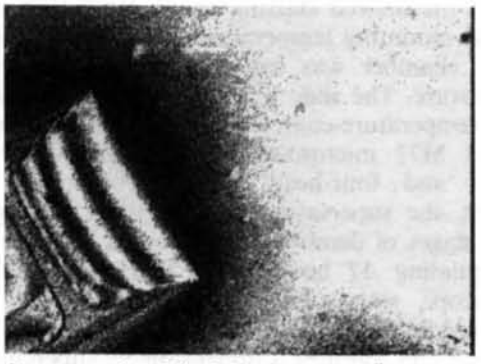

Fig. 4. Same crystal as Fig. 3, 8 s later. Long direction is [010]. The area furthest from the crystal is the region of highest concentration. The long dimension of the photograph equals 0.54 mm.

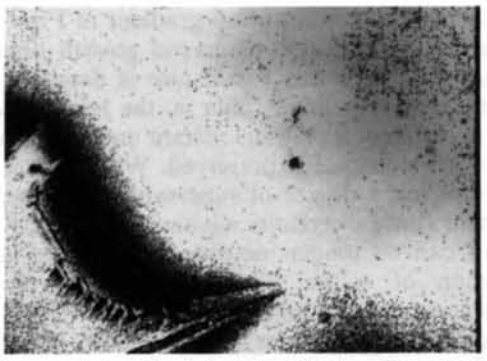

Fig. 5. Same crystal as Fig. 4, 4 s later. The long dimension of the photograph equals 0.54 mm.

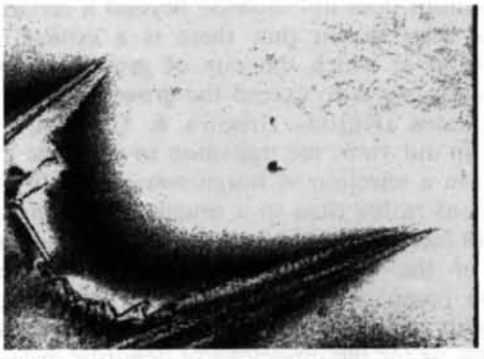

Fig. 6. Same crystal as Fig. 5, 0.2 s later. The long dimension of the photograph equals 0.54 mm. The growth velocity of the needle tip = 0.33 mm s^{-1}; the growth velocity of the (010) face = 0.05 mm s^{-1}.

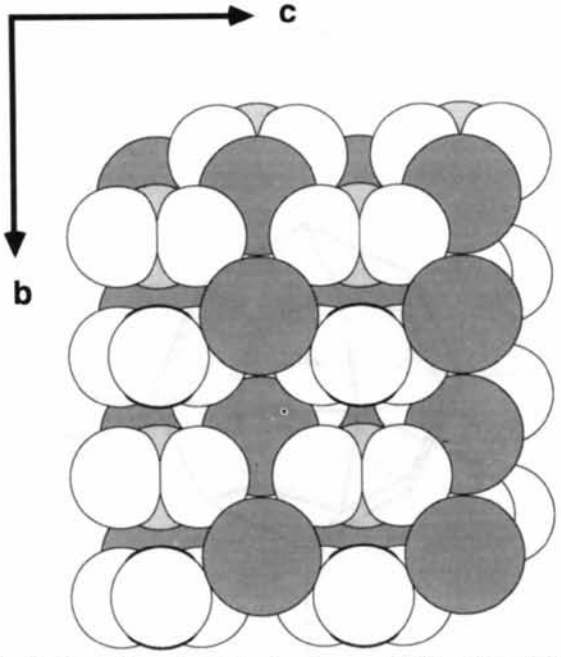

Fig. 7. Projection of KNO_3 structure on (100), after Wyckoff (1964). Open circles are oxygen, large shaded circles are potassium.

Table 1. KNO_3 *plane spacings*

hkl	Spacing (Å)	Form observed (Groth, 1908)
100	9.17	Yes
010	6.43	Yes
001	5.42	Yes
110	5.26	Yes
101	4.66	Yes
011	4.14	No
111	3.77	Yes
210	3.73	Yes
201	3.50	No
211	3.07	No
120	3.03	Yes
021	2.76	No
310	2.76	No
301	2.66	No
121	2.65	No
102	2.60	No
012	2.50	No
311	2.46	No
112	2.41	No
221	2.37	No
320	2.21	No
212	2.19	No
410	2.16	No
401	2.11	No
130	2.09	No
321	2.05	No
302	2.03	No
122	2.02	No
411	2.01	No
031	1.99	No
⋮	⋮	⋮
041	1.54	No
⋮	⋮	⋮
051	1.25	No

became distorted. As a result, the new needle crystal tip found itself in a region of high concentration, which further enhanced is growth rate.

Mechanisms of crystal growth

The foregoing observations can be understood by considering the mechanism by which solute is added to a growing crystal. The faces that bound a well developed faceted crystal are perpendicular to the slowest-growing directions. This idea is further elaborated in the Bravais–Donnay–Harker rule, that 'the relative importance of the faces of a crystal is directly proportional to the interplanar spacings of the parallel lattice planes' (Azaroff, 1975). As Table 1 shows, KNO_3 crystals conform closely to this rule; the discrepancies represented by (011), (201) and (211) are not surprising in view of the limitations of the Bravais–Donnay–Harker rule (Schneer, 1983). Fig. 8 illustrates a KNO_3 crystal and shows some of these directions and the interfacial angles. This reasoning applies rigourously, of course, only to nondirectional bonding, as in metals.

The reason that differential growth rates are related to plane spacing is that the 'roughness' of a face, related to the reticular density of lattice points on that face, determines the energetics and kinetics

of addition of solute to that face (Azaroff, 1975). Planes with large interplanar spacing have high reticular density and are, therefore, inhospitable to the incorporation of new solute. Indeed, such planes can add material only at screw dislocations. In contrast, rough planes can grow by the addition of material anywhere on the surface and, thus, grow more rapidly at a given supersaturation. The result of this difference in growth rate is that faster growing directions become edges and corners, leaving the slower directions as bounding planes.

There is a body of experimental and theoretical work supporting the existence of a 'roughening transition', which affects the mechanism of crystal growth (Bennema & van der Eerden, 1987). This transition has been used to explain the transition from faceted to dendritic habit (Sunagawa, 1981, 1987). We propose a somewhat different explanation for the change in habit in KNO_3.

As the temperature is lowered, beginning with Fig. 3, the solution becomes increasingly unstable. The rate of deposition of solute increases, as shown by the steepening concentration gradient in Figs. 3 and 4. As long as the various crystal growth directions can accommodate this higher rate of deposition, the growth process is linear: that is, the relative growth rates in different directions remain unchanged, so the shape of the crystal is preserved. With further cooling, however, a degree of supersaturation is reached at which those directions advancing by screw dislocations can no longer increase their rate of accommodation of solute. The excess solute therefore deposits on rougher higher index planes – (031) (041) and (051) – which can accommodate still higher deposition rates: growth in these directions is enhanced, as seen in Fig. 5. [While it may be an overstatement to say that the growth rate at screw dislocations does not increase beyond a certain rate, it has been shown that there is a critical supersaturation at which the rate of growth by surface nucleation starts to exceed the growth rate at screw dislocations (Kuroda, Irisawa & Ookawa, 1987).] Thus, in our view, the transition to dendritic growth is due to a selection of rough *versus* smooth growth directions rather than to a roughening of previously smooth faces. It should be noted that the mechanistic view of the transition from normal to dendritic growth complements the bulk view of the surface instability (Mullins & Sekerka, 1963, 1964) by accounting for the directions of dendritic growth.

The preferential deposition of solute at these protruding corners naturally causes a change in the shape of the diffusion field, since more rapid solute

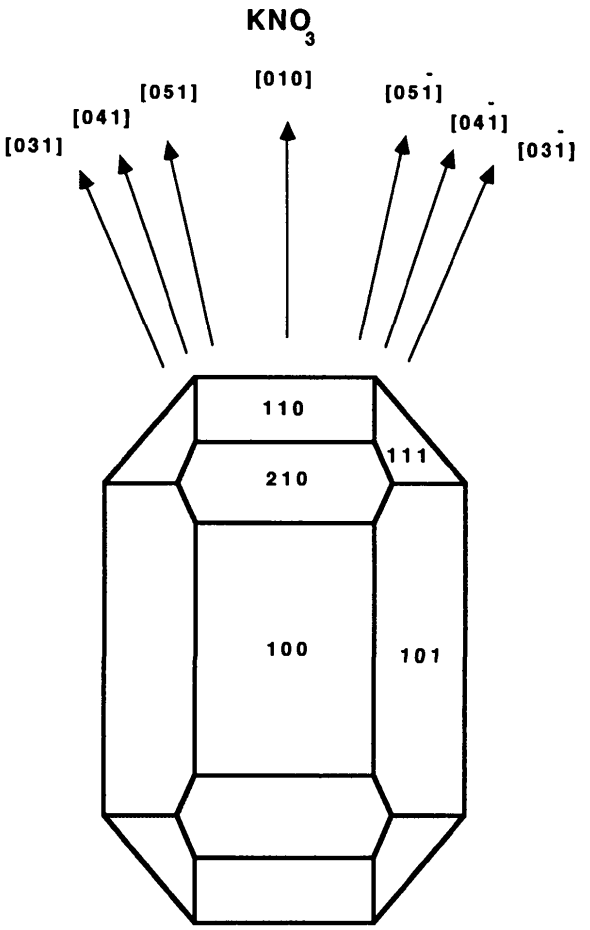

Fig. 8. Projection of KNO_3 crystal on (100).

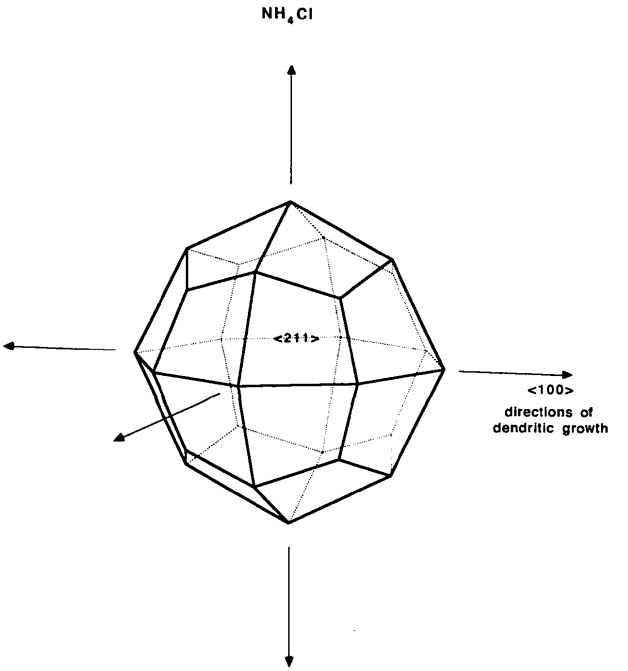

Fig. 9. Faceted crystal of NH_4Cl, after Groth (1906).

Table 2. KNO_3 *Interfacial angles*

$[hkl]_1$	$[hkl]_2$	Calculated angle (°)	Observed sidebranch angle (°)
031	$03\bar{1}$	43.2	42 ± 0.6
031	$04\bar{1}$	38.1	38 ± 0.6
031	$05\bar{1}$	34.9	35 ± 0.6
010	031	21.6	22 ± 0.6
010	041	16.5	17 ± 0.6

deposition is now occurring at these locations. As Figs. 5 and 6 show, this distortion of the diffusion field places the new growth direction in a region of higher concentration than had been the case when the crystal was growing normally (*cf.* Figs. 3 and 4). This proximity to a solution of high concentration further accelerates growth in this new direction. Chan, Reimer & Kahlweit (1976) commented on this interaction between the diffusion field and crystal protrusions in the case of NH_4Cl. Thus, there is a positive feedback between exaggerated corner growth and the supply of solute to the needle crystal. This positive feedback is analogous to the autocatalysis associated with pattern formation in chemical reaction systems (Scott & Showalter, 1992). The point of instability of normal growth would be the growth rate at which those faces growing by screw dislocations cannot add solute any faster and are overtaken by deposition at faces growing by nucleation.

For KNO_3, the quantitative agreement between the measured sidebranch angles and the calculated interfacial angles for faces of low reticular density supports this view (Table 2). It is also relevant to note that in NH_4Cl, a frequent subject of dendrite research, the direction of dendritic growth is ⟨100⟩, ⟨110⟩ or ⟨111⟩ (Chan, Reimer & Kahlweit, 1976), none of which are faces in normal NH_4Cl crystals, as shown in Fig. 9 (Groth, 1906). Furthermore, when NH_4Cl dendrites are partially redissolved and then regrown normally at low supersaturation, the previous points of attachment of the sidebranches grow out to become corners (Fig. 10); this observation shows that the direction of dendrite growth corresponded to a rapidly growing direction in the normal crystal. Finally, dendritic snowflakes originating from tabular hexagonal crystals invariably develop the dendritic protrusions at the corners of the hexagons (Bentley & Humphreys, 1962). These observations indicate that, at least in these cases, the transition from faceted to dendritic habit is caused not by a change in the growth mechanism occurring at any particular face, but rather by a change in preferential deposition of solute at faces which are already growing by a different mechanism.

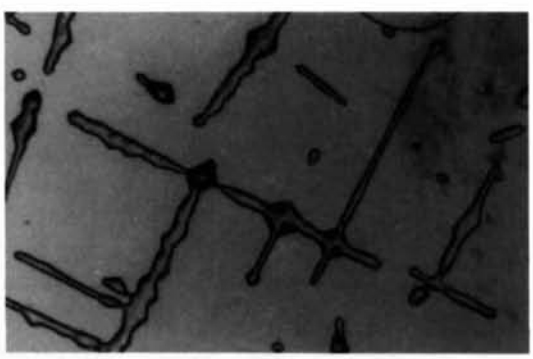

Fig. 10. NH_4Cl crystal grown initially as a dendrite at 291 K, then annealed at 293 K for 4 days. Note the development of polyhedral crystals at the intersections of dendrite branches. Compare these polyhedra with Fig. 9. The long dimension of the photograph equals 3.0 mm.

The authors are grateful to The Research Corporation and to the Simmons College Fund for Research for support of this work. We thank a referee for bringing special aspects of the Bravais–Donnay–Harker rule to our attention.

References

AZAROFF, L. V. (1975). *Introduction to Solids*, pp. 142–143. Huntington, USA: Robert E. Krieger.

BEN-JACOB, E., GOLDENFELD, N., LANGER, J. S. & SCHÖN, G. (1983). *Phys. Rev. Lett.* **51**, 1930–1932.

BENNEMA, P. & EERDEN, J. P. VAN DER (1987). In *Morphology of Crystals*, Part A, pp. 1–75, edited by I. SUNAGAWA. Boston: D. Reidel.

BENTLEY, W. A. & HUMPHREYS, W. J. (1962). *Snow Crystals*. New York: Dover Publications.

CHAN, S.-K., REIMER, H.-H. & KAHLWEIT, M. (1976). *J. Cryst. Growth*, **32**, 303–315.

CLASSEN, A., MISBAH, C., MÜLLER-KRUMBHAAR, H. & SAITO, Y. (1991). *Phys. Rev. A*, **43**, 6920–6933.

DOUGHERTY, A., KAPLAN, P. D. & GOLLUB, J. P. (1987). *Phys. Rev. Lett.* **58**, 1652–1655.

FIELD, R. J. & BURGER, M. (1985). *Oscillations and Traveling Waves in Chemical Systems*. New York: John Wiley.

GROTH, P. (1906). *Chemische Krystallographie*, Vol. 1, pp. 182–183. Leipzig: Wilhelm Engelman.

GROTH, P. (1908). *Chemische Krystallographie*, Vol. 2, p. 74. Leipzig: Wilhelm Engelman.

KURODA, T., IRISAWA, T. & OOKAWA, A. (1987). In *Morphology of Crystals*, Part B, pp. 591–612, edited by I. SUNAGAWA. Boston USA: D. Reidel.

LANGER, J. S. (1980). *Rev. Mod. Phys.* **52**, 1–28.

LANGER, J. S. (1989). *Science*, **243**, 1150–1156.

LANGER, J. S. (1992). *Phys. Today*, **45**(10), 24–31.

MULLINS, W. W. & SEKERKA, R. F. (1963). *J. Appl. Phys.* **34**, 323–329.

MULLINS, W. W. & SEKERKA, R. F. (1964). *J. Appl. Phys.* **35**, 444–451.

NICOLIS, G. & PRIGOGINE, I. (1977). *Self-Organization in Non-Equilibrium Systems*. New York: John Wiley.

SCHNEER, C. J. (1983). In *Crystallography in North America*, pp. 380–388, edited by D. MCLACHLAN JR & J. GLUSKER. New York: American Crystallographic Association.

SCOTT, S. K. & SHOWALTER, K. (1992). *J. Phys. Chem.* **96**, 8702–8711.

SOLTZBERG, L. J., FAPPIANO, S. A., HIDEK, L. E., O'BRIEN, M. J. & SUAREZ, L. L. (1992). *Acta Cryst.* A**48**, 457–461.
SUNAGAWA, I. (1981). *Bull. Miner.* **104**, 81–87.
SUNAGAWA, I. (1987). In *Morphology of Crystals*, Part B, pp. 509–587, edited by I. SUNAGAWA. Boston: D. Reidel.
THOMPSON, D. (1961). *On Growth and Form*, abridged ed. by J. T. BONNER. Cambridge: Cambridge University Press.
THOMPSON, J. M. T. & STEWART, H. B. (1986). *Nonlinear Dynamics and Chaos*. New York: John Wiley.
WINCHELL, A. N. & WINCHELL, W. (1964). *The Microscopical Characters of Artificial Inorganic Solid Substances*, p 101. New York: Academic Press.
WYCKOFF, R. G. (1964). *Crystal Structures*, 2nd ed., Vol. 2, pp. 364–365. New York: Interscience.

Acta Cryst. (1994). **B50**, 524–538

Crystal Chemistry and Structures of Lead–Antimony Sulfides

BY ANICETA SKOWRON AND I. DAVID BROWN

Institute for Materials Research, McMaster University, Hamilton, Ontario, Canada L8S 4M1

(*Received* 6 *April* 1993; *accepted* 2 *March* 1994)

Abstract

Using chemical and topological rules to describe the structural chemistry of Pb^{2+} and Sb^{3+}, we show that the substitution of Sb^{3+} into PbS (galena) results in four possible topological series of structures, and that the conflicting requirements of chemical bonding and charge neutrality severely limit the number of structures that can occur in each series. The model accounts for the existence of most of the compounds found in the pure Pb–Sb–S phase diagram. It correctly predicts the distribution of Pb^{2+} and Sb^{3+} over the various cation sites and shows why the mirror plane is lost in some phases.

1. Introduction

Lead and antimony are widely found in nature in the form of sulfides and many different mineral forms have been reported (Craig, Chang & Lees, 1973). Most of the minerals contain impurities and, in many cases, these impurities are important in stabilizing structures that would not be stable in the pure Pb–Sb–S system. For example, the plagionite group of minerals: semseyite, heteromorphite, plagionite and füllopite, which have also been obtained in hydrosynthesis experiments at temperatures near 673 K (Robinson, 1948; Jambor, 1968), fail to appear in the dry system. Heating experiments on natural and synthetic compounds of this group cause their decomposition to phases stable in the dry system. This may indicate, as suggested by Garvin (1973), that the plagionite group minerals contain an additional essential component, probably hydrogen, liberated during heating. In this paper, we confine ourselves to the dozen or so compounds known to occur in the pure ternary system.

The dry PbS–Sb_2S_3 system has been the subject of several experimental studies (Garvin, 1973; Craig *et al.*, 1973; Hoda & Chang, 1975; Salanci & Moh, 1970; Wang, 1976; Salanci, 1979; Bortnikov Nekrasov, Mozgova & Tsepin, 1981). Salanci (1979) has published a phase diagram, an adapted form of which, shown in Fig. 1, indicates six ternary compounds between PbS and Sb_2S_3: II = $Pb_7Sb_4S_{13}$, III = $Pb_3Sb_2S_6$, IV = boulangerite, $Pb_5Sb_4S_{11}$, V =

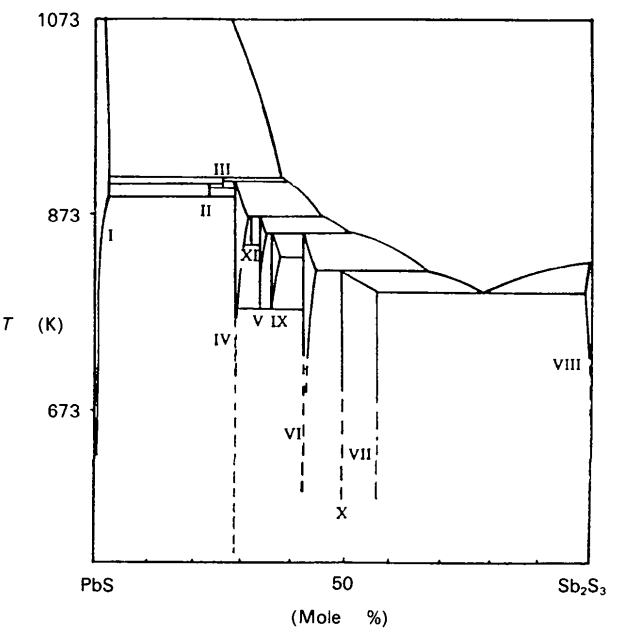

Fig. 1. Schematic phase diagram of the PbS–Sb_2S_3 system after Salanci (1979). The phases are I, galena; II, $Pb_7Sb_4S_{13}$; III, $Pb_3Sb_2S_6$; IV, boulangerite; V, $Pb_2Sb_2S_5$ (monoclinic); VI, robinsonite; VII, zinckenite; VIII, stibnite; IX, $Pb_5Sb_6S_{14}$; X, $PbSb_2S_4$; XI, $Pb_7Sb_6S_{16}$.

©1994 International Union of Crystallography
Printed in Great Britain – all rights reserved